Journal of
Ceramic Science
and Technology

J. Ceram. Sci. Tech., **06** [02] 141-146 (2015)
DOI: 10.4416/JCST2015-00013
available online at: http://www.ceramic-science.com

3D Printing of Porous Al_2O_3 and SiC ceramics

C. Polzin*[1], D. Günther[2], H. Seitz[1]

[1]Fluid Technology and Microfluids, University of Rostock,
Justus-von-Liebig-Weg 6, D-18059 Rostock, Germany
[2]Paul-Lenz-Straße 1a, D-86316 Friedberg, Germany

received March 27, 2015; received in revised form May 5, 2015; accepted May 12, 2015

Abstract

We demonstrated the possibility to fabricate porous ceramics made of alumina and silicon carbide by means of 3D printing. For this investigation, two ceramic powder blends, VX-AlOx-Typ A and VX-SiC-Typ A, were used. Several specimens were printed, sintered and characterized. The specimens possess high porosity of up to 69 % for alumina and 55 % for silicon carbide. The compressive strength amounted to 6.8 MPa for the VX-AlOx-Typ A and to 19.65 MPa for the VX-SiC-Typ A specimens. The flexural strength amounts to 4.17 MPa and 9.74 MPa for the alumina and silicon carbide parts respectively. The thermal expansion coefficient for parts made of VX-AlOx-Typ A is 1.03x10^{-6} K^{-1} and for parts made of VX-SiC-Typ A it is 6.87x10^{-6} K^{-1}.

Keywords: Porous ceramic, alumina, silicon carbide, 3D printing, additive manufacturing.

I. Introduction

The manufacturing of complex ceramic parts with defined microstructure is a challenge today. With regard to this issue, additive manufacturing technology is a promising alternative to conventional manufacturing procedures [1]. Various additive manufacturing technologies like stereolithography (SLA), selective laser sintering (SLS), fused deposition modeling (FDM), laminated object manufacturing (LOM) and three-dimensional printing (3D printing) have already been used to manufacture various ceramics or ceramic green bodies [2, 3, 4, 5]. One of the fastest and most cost-efficient technologies is 3D printing. Here ceramic powder materials are deposited in layers and selectively joined with binder from an inkjet print head [6]. 3D printing has already been used to manufacture both bioceramics and technical ceramics [7, 8, 9]. Especially in the field of bioceramics, various processing aspects of powder-based 3D printing process have been investigated to date [10, 11, 12, 13].

Alumina and silicon carbide are some of the most promising technical ceramic materials today. In this study, the processing of two new ceramic powder blends based on alumina and silicon carbide on a 3D printer was investigated. These powder blends were basically developed for direct manufacturing of porous ceramic components like oven insulations, hot gas filters, catalyst carriers and other technical ceramics. 3D-printed specimens made from these powder blends were characterized in terms of their mechanical properties, porosity and thermal expansion.

* Corresponding author: christian.polzin@uni-rostock.de

II. Materials and Methods

(1) Ceramic blends

For this investigation, two ceramic blends provided by Voxeljet AG (Augsburg, Germany) were used. The *VX-SiC-Typ A* is a bimodal ceramic mixture based on silicon carbide and a soluble polymer granulate with a mean grain size of 50 µm. *VX-AlOx-Typ A* is a mixture of alumina, feldspar and a soluble polymer granulate. The mean grain size of both materials is 50 µm.

(2) Binder

Solupor-Binder (Voxeljet, Augsburg, Germany) was used as binder fluid. The binder partially dissolves the polymeric fraction of the ceramic blends and the ceramic particles glue together.

(3) 3D printing

The silicon carbide and alumina green parts were manufactured using a 3D printer VX500 (Voxeljet Technology GmbH, Augsburg, Germany). The job box has the dimensions (xyz) 500 x 400 x 300 mm. The job box filled with the ceramic blends is printed with the binder layer by layer. The volume fraction of solvent after printing is 26.05 % for the VX-AlOx-Typ A and 8.8 % for the VX-SiC-Typ A respectively.

The STL files of the parts to be printed are imported into the machine software Rapix3D (Forwiss, Passau, Germany) and positioned in the virtual job box.

After completion of the job, the parts were removed from the job box, cleaned with an air blower, and dried for 24 h in an oven at 40 °C.

(4) Test parts

The following test parts were designed (Table 1):

Table 1: Test parts and dimensions.

Name	Dimension	Test
Bending test bar	4x10x80 mm (w x h x l)	Bending stress measurement
Cylinder	∅ 10 mm, height 10.5 mm	Compressive stress measurement
Cylinder	∅ 5 mm, height 10 mm	Thermal expansion measurement
Cylindrical plate	∅ 13 mm, height 5 mm, central hole with ∅ 1 mm	Porosity measurement

All parts were designed in the CAD tool SolidWorks (Concord, USA) and were exported as an STL file and checked for failures in Magics (Materialise Group, Leuven, Belgium).

(5) Sintering

Liquid phase sintering was applied to sinter the VX-AlOx-Typ A parts at 1200 °C for 3 h under atmosphere. The heating rate was 5 K/min. The parts made of VX-SiC-Typ A were recrystallization-sintered up to a temperature of 2200 °C in argon atmosphere [14, 15].

(6) Characterization

The shrinkage of the green parts and the sintered parts was determined with a digital caliper at the bending test bar. A uniaxial testing system Zwick (Zwick GmbH&Co.KG, Ulm, Germany) with a 5 kN load cell was used for the mechanical characterization of the green parts and the sintered parts. The compressive strength was measured on five cylindrical parts with a diameter of 10 mm and a height of 10 mm. The flexural strength was characterized on five bending test bars with a three-point bending test with a support distance of 40 mm. The open porosity was determined with the Archimedes method using distilled water as immersion fluid. A Lauda TD 1 C tensiometer (LAUDA GmbH&Co. KG) was used for the immersion weighing. The determination of the specific surface area with gas adsorption (BET) method was performed with an ASAP 2020 (Micromeritics, Norcross, USA). Thermal expansion was measured with a push-rod dilatometer. The heating rate was 5 K/min and the maximum temperature was limited to 990 °C. According to Fig. 1, three measurement cycles were conducted. The SEM images were obtained with a Zeiss DSM 960 A (Carl Zeiss AG).

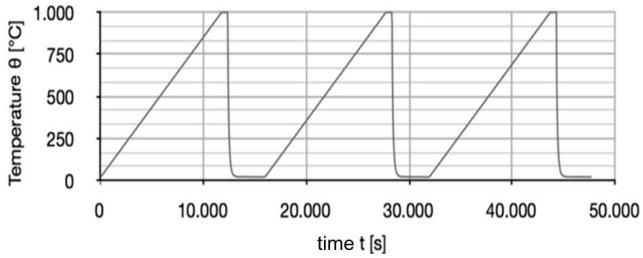

Fig. 1: Heating procedure for the thermal expansion test.

To verify the porosity measurements, microsections were prepared and investigated. Micro-CT images were obtained with a Micro-CT SkyScan 1172 (Bruker microCT, Kontich, Belgium).

III. Results

(1) Shrinkage

Isotropic shrinkage in all three dimensions could be observed. The linear shrinkage was calculated from the length of the bending test bars before and after sintering. The results of the shrinkage measurements are displayed in Table 2.

(2) Mechanical characterization

The test parts were successfully printed and sintered. The maximum compressive strength of the VX-AlOx-Typ A green parts is 5.89 ± 0.09 MPa. The 3D-printed green parts made of the VX-SiC-Typ A have a maximum compressive strength of 2.64 ± 0.4 MPa. As a result of the sintering process, the compressive strength could be increased up to 6.80 ± 0.26 MPa for the VX-AlOx-Typ A and up to 19.65 ± 1.77 MPa for the VX-SiC-Typ A (Fig. 2).

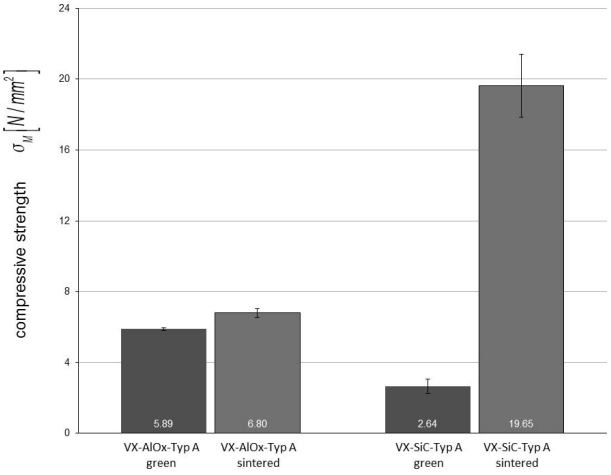

Fig. 2: Compressive strength of the AlOx- and SiC- specimens.

Table 2: Results of the shrinkage measurement.

	Green	Shrinkage green to CAD	Sintered	Shrinkage sintered to green	Shrinkage sintered to CAD
VX-AlOx-Typ A	79.48±0.12 mm	0.65 %	75.86±0.31 mm	4.55 %	5.18 %
VX-SiC-Typ A	79.32±0.11 mm	0.51 %	79.17±0.28 mm	0.52 %	1.04 %

The maximum flexural strength for the 3D-printed VX-AlOx-Typ A green parts is 2.91 ± 0.9 MPa. The VX-SiC-Typ A green parts have a maximum flexural strength of 1.99 ± 0.18 MPa. As a result of the sintering process, the flexural strength could be increased up to 4.17 ± 0.5 MPa for the VX-AlOx-Typ A and up to 9.74 ± 0.96 MPa for the VX-SiC-Typ A (Fig. 3).

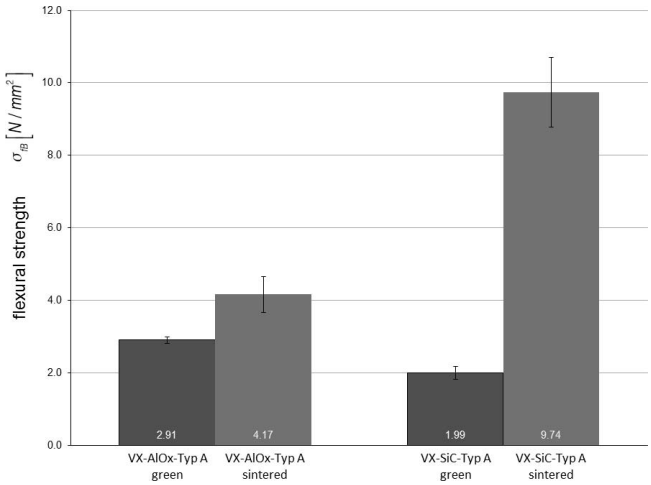

Fig. 3: Flexural strength of the AlOx- and SiC-specimens.

The elongation at break of the alumina parts decreased significantly from 1.53 % to 0.44 % after sintering (Fig. 4). Since silicon carbide green parts feature a relatively low elongation at break after 3D printing, only a minor decrease from 0.44 % to 0.26 % could be determined (Fig. 4).

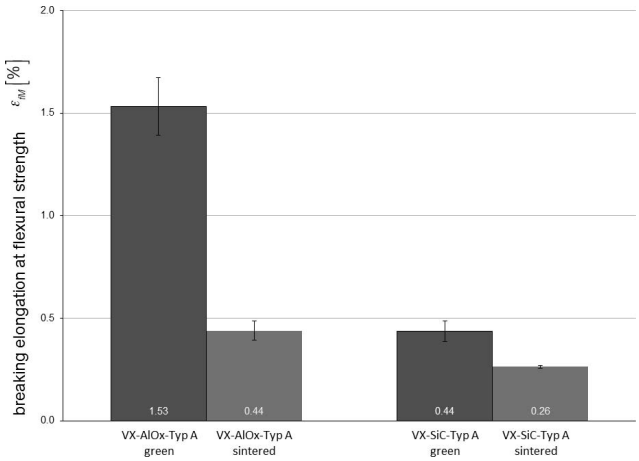

Fig. 4: Elongation at break.

(3) SEM analysis

Fig. 5 shows the SEM analysis of the ceramic green part made of VX-AlOx-Typ A. Different components of the blend can be identified. The spherical particles are the soluble polymer granules. The irregular particles of the same sizes are the alumina granules. The small particles on the soluble polymer granules and on the alumina granules are the feldspar component.

Sintered specimens made of VX-AlOx-Typ A are shown in Fig. 6. The feldspar component formed interconnections between the alumina granules during liquid phase sintering. Additionally, it is obvious that not all alumina particles are connected to each other. The polymer granules are completely pyrolyzed.

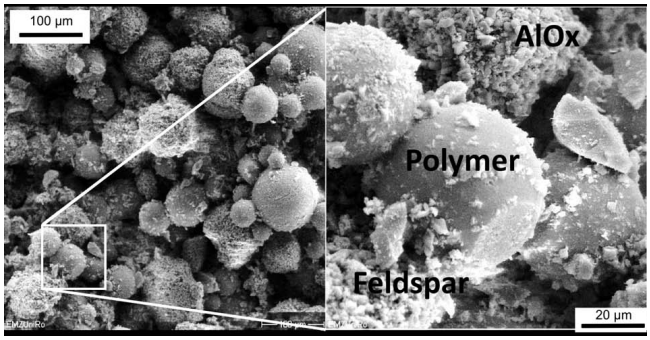

Fig. 5: SEM image of a green part made of VX-AlOx-Typ A; 200 x and 1000 x magnification.

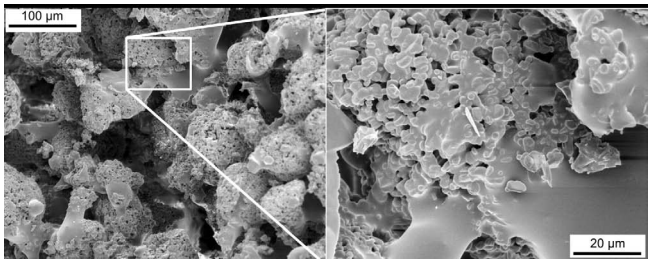

Fig. 6: SEM image of a sintered specimens made of VX-AlOx-Typ A; 200 x and 1000 x magnification.

Fig. 7 shows the VX-SiC-Typ A green part. In comparison with the VX-AlOx-Typ A, it can be seen that the soluble polymer granulate has completely dissolved during the printing process. In this figure only the bimodal mixture of bigger silicon carbide granules as the base component and smaller silicon carbide granules for increasing the packing density are visible.

After recrystallization sintering, the typical grain growth and the sintering connections of the silicon carbide granules are visible (Fig. 8).

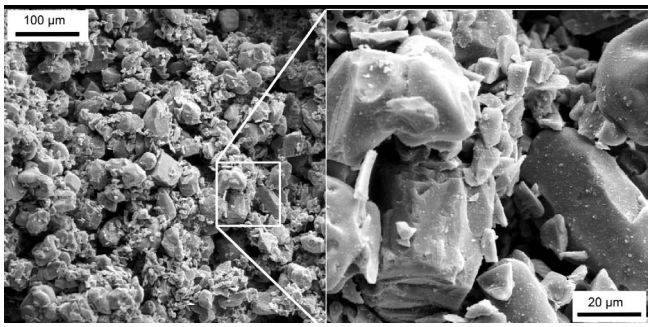

Fig. 7: SEM image of a green part made of VX-SiC-Typ A; 200 x and 1000 x magnification.

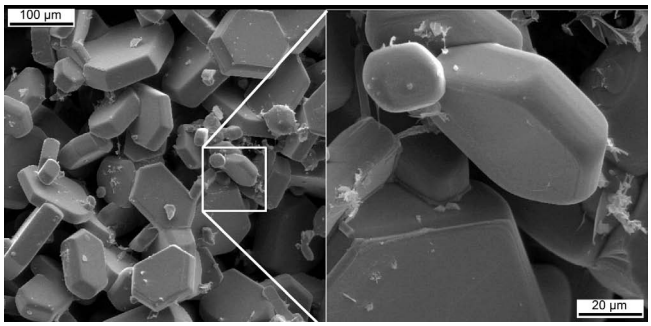

Fig. 8: SEM of sintered SiC; 200 x and 1000 x magnification, sintered.

(4) Porosity measurement

The measurement of porosity leads to following results (Fig. 9)

The sintered parts made of VX-AlOx-Typ A have a true porosity of 69.6 ± 0.21 % with an amount of 69.3 ± 0.27 % open pores and 0.3 ± 0.20 % closed pores. The test pieces made of VX-SiC-Typ A have a true porosity of 55.5 ± 0.17 % with an amount of 48.7 ± 0.33 % open pores and 6.8 ± 0.43 % closed pores.

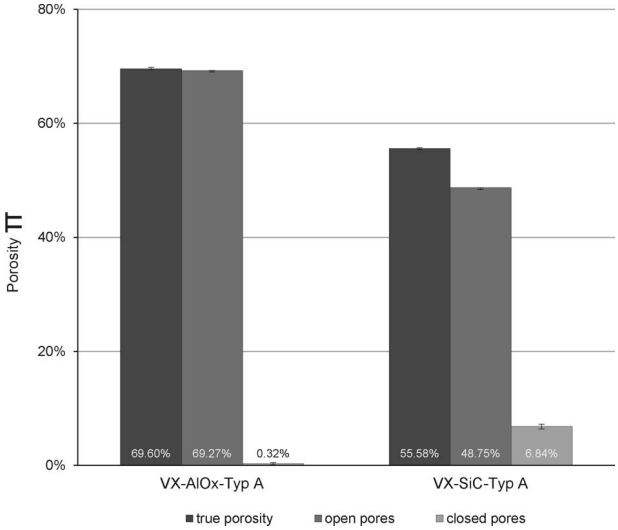

Fig. 9: Porosity measurement.

(5) Coefficient of thermal expansion

Figs. 10 and 11 illustrate the elongation in dependence on the temperature. For the alumina sample, a negative elongation is significant over the three heating cycles. Between 900 °C and the maximum temperature of 990 °C the nearly linear elongation changes. At this temperature, the elongation decreases rapidly with rising temperature. During the holding time of 16 minutes at maximum temperature, shrinkage is visible at each cycle. The thermal expansion coefficient for the VX-AlOx-Typ A parts between 0 °C and 990 °C is $\alpha = (1.03 \pm 0.06) \times 10^{-6} K^{-1}$.

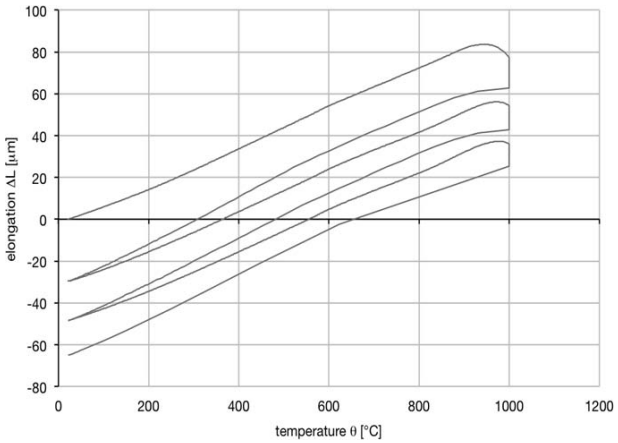

Fig. 10: Measurement of thermal expansion coefficient for VX-AlOx-Typ A.

The measurement of elongation while heating up the silicon carbide samples shows a more linear trend. Between each cycle, a slight misalignment is visible. The thermal expansion coefficient for the VX-SiC-Typ A parts between 0 °C and 990 °C is $\alpha = (6.87 \pm 0.36) \times 10^{-6} K^{-1}$.

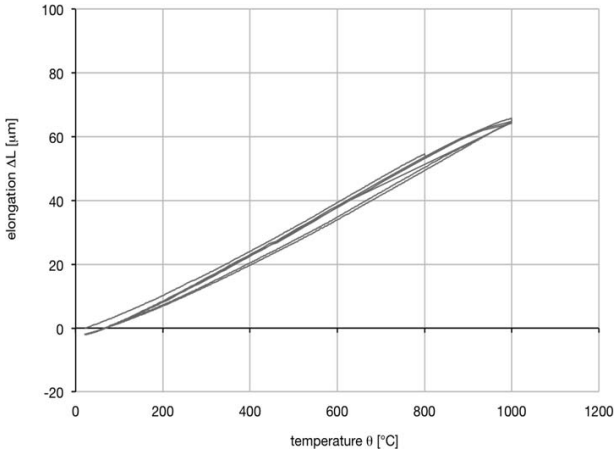

Fig. 11: Measurement of thermal expansion coefficient for VX-SiC-Typ A.

IV. Discussion

The 3D-printed green parts are stable and exhibit sufficient mechanical strength for safe handling. Furthermore, the 3D-printed parts do not lose their contour when they are unpacked and placed in the sintering furnace. The polymer fraction in the powder blends VX-AlOx-Typ A and VX-SiC-Typ A leads to maximum breaking elongation of 1.53 % and 0.44 % respectively for the green parts. As a result of sintering, the flexural strength increased slightly in comparison to the green part. For the AlOx parts, only the interconnections of feldspar are now responsible for the mechanical strength. Owing to the fluid phase sintering process, the shrinkage of parts made of VX-AlOx-Typ A is higher than the shrinkage of the SiC parts. The recrystallization-sintered SiC parts have almost no shrinkage. Looking at the SEM images, only a few of these interconnections are visible. Furthermore, the high true porosity and the high amount of open pores are a good indication that the alumina granules are partly connected.

The results of the measurement of the thermal expansion coefficient indicate the tendency of the parts to creep at temperatures above 950 °C. It can be supposed that the pressure on the test specimen owing to the initial tension of fixation in the push-rod dilatometer and the high temperature close to the melting point of feldspar lead to this creep. AlOx parts feature a sintering shrinkage of 4.55 %. It is possible to compensate for this shrinkage by scaling the CAD file before 3D printing.

The flexural strength of the green parts made of silicon carbide is lower than the strength of the alumina green parts. This lower strength is owed to the lower amount of polymeric fraction in the ceramic mixture. Anyway, the strength is sufficient to unpack the parts and clean them to remove the excessive powder. Owing to the low polymeric fraction content, the maximum elongation at break is lower than the elongation of the alumina green parts too. As a result of sintering, the flexural strength increased up to 5.7 times to a maximum of 10.8 MPa. The low maximum elongation at break of 0.36 % proves that the sintered parts are brittle. The high porosity and the open structural condi-

tions visible in the SEM images leads to the assumption of a high notch effect while bending. The results of the measurement of the thermal expansion coefficient indicate the thermal stability of the ceramics at temperatures of 990 °C. Liquid phase sintering of the SiC parts leads to a very low sintering shrinkage of 0.52 %, which is favorable for the production of parts with high dimensional accuracy.

3D-printed porous Al_2O_3 and SiC ceramics cannot achieve the mechanical properties of their dense counterparts. In addition to the high porosity, the typically high surface roughness of 3D-printed ceramic (see Figs. 12 and 13) has major effects on the mechanical properties.

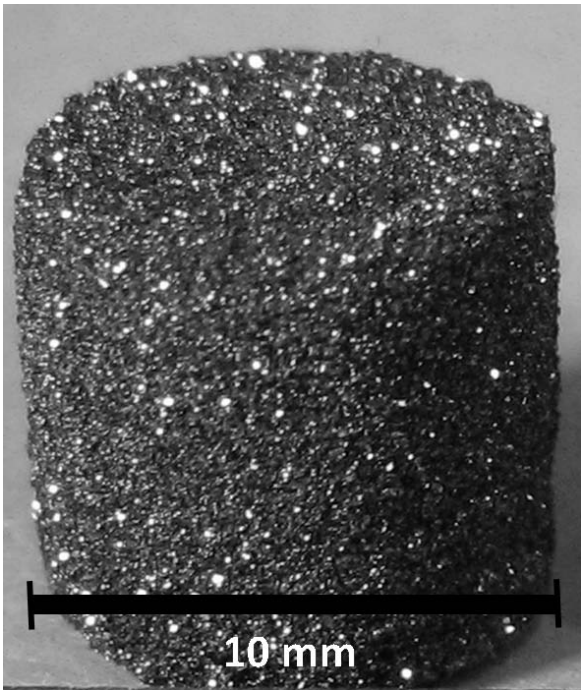

Fig. 12: SiC specimen for compressive strength testing.

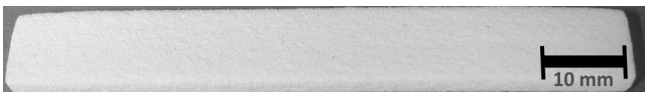

Fig. 13: AlOx specimen for the bending test.

Only isotropic mechanical properties could be detected. The anisotropic crystal elastic behavior of the single ceramic grains has no influence on the macroscopic mechanical properties since the grains have no preferred orientation in the bulk ceramic.

V. Conclusions

This investigation demonstrated the possibility to manufacture complex porous ceramic parts with a 3D printer using the powder blends VX-SiC-Typ A and VX-AlOx-Typ A. The parts are highly porous and feature high thermal shock resistance. Accordingly, the ceramics can be used for catalytic, filtration or high-temperature applications. Especially parts made of VX-AlOx-Typ A with an amount of open pores of 69.27 % could be interesting for filtration applications. The 3D-printed specimens featured very high contour stability. However, the contour stability of more complex and filigree parts has to be investigated. Further studies will also focus on the analysis and optimization of the pore size and pore size distribution for specific applications. On the other hand, future work will investigate the possibilities of manufacturing nearly dense parts by using different infiltration procedures. These parts would have increased mechanical properties and could make this material interesting for a wider field of applications. The VX-SiC-Typ A is an interesting ceramic especially for high-temperature applications.

References

1 Hammel, E., Ighodaro, O.L.-R., Okoli, O.I.: Processing and properties of advanced porous ceramics: an application based review, *Ceram. Int.,* **40**, [10], 15351 – 15370, (2014).

2 Cawley, J.D.: Solid freeform fabrication of ceramics, *Curr. Opin. Solid St. M.,* **4**, 483 – 489, (1999).

3 Halloran, J.W., Tomeckova, V., Gentry, S.: Photopolymerization of powder suspensions for shaping ceramics, *J. Eur. Ceram. Soc.*, **31**, [14], 2613 – 2619, (2011).

4 Balla, V.K., Bose, S., Bandyopadhyay, A.: Processing of bulk alumina ceramics using laser engineered net shaping, *Int. J. Appl. Ceram. Tec.*, **5**, [3], 234 – 242, (2008).

5 McNulty, T.F., Mohammadi, F., Bandyopadhyay, A., Shanefield, D.J., Danforth, S.C., Safari, A.: Development of a binder formulation for fused deposition of ceramics, *Rapid Prototyping J.*, **4**, [4], 144 – 150, (1998).

6 Sachs, E., Cima, M., Williams, P., Brancazio, D., Cornie, J.: Three dimensional Printing: rapid tooling and prototypes directly from a CAD model, *J. Eng. Ind.,* **114**, 481 – 488, (1992).

7 Yin, X., Travitzky, N., Greil, P.: Near-Net-shape fabrication of Ti_3AlC_2-based composites, *Int. J. Appl. Ceram. Tec.*, **4**, [2], 184 – 190, (2007).

8 Fu, Z., Schlier, L., Travitzky, N., Greil, P.: Three-dimensional printing of SiSiC lattice truss structures, *Mater. Sci. Eng. A*, **560**, 851 – 856, (2013).

9 Butscher, A., Bohner, M., Hofmann, S., Gauckler, L., Müller, R.: Structural and material approaches to bone tissue engineering in powder-based three-dimensional printing, *Acta Biomaterialia,* **7**, [3], 907 – 920, (2011).

10 Butscher, A., Bohner, M., Roth, C., Ernstberger, A., Heuberger, R.: Printability of calcium phosphate powders for three-dimensional printing of tissue engineering scaffolds, *Acta Biomater.*, **8**, 373 – 385, (2012).

11 Spath, S., Seitz, H.: Influence of grain size and grain-size distribution on workability of granules with 3D printing, *Int. J. Adv, Manuf. Technol.,* **70**, 135 – 144, (2014).

12 Farzadi, A., Solati-Hashjin, M., Asadi-Eydivand, M., Abu Osman, N.A.: Effect of layer thickness and printing orientation on mechanical properties and dimensional accuracy of 3D printed porous samples for bone tissue engineering, *PloS One*, **9**, [9], (2014).

13 Suwanprateeb, J., Sanngam, R., Panyathanmaporn, T.: Influence of raw powder preparation routes on properties of hydroxyapatite fabricated by 3D printing technique, *Mater. Sci. Eng. C*, **30**, [4], 610 – 617, (2010).

14 Bingquan, H., Wenting, C., Yang, Z.: The improvement method design for beta-SiC recrystallization, *Appl. Mech. Mater.,* **55 – 57**, 578 – 581, (2011).

15 RongZhen, L., Bo, W., JiKuan, C., JianFeng, Y., JiQiang, G.: A novel method for the preparation of porous SiC, *Mater. Sci. Forum,* **620 – 622**, 773 – 776, (2009).